Unveiling linearly and nonlinearly correlated signals between gravitational wave detectors and environmental monitors

Hirotaka Yuzurihara,[1,*] Kazuhiro Hayama,[2,3] Shuhei Mano,[4] Didier Verkindt,[5] and Nobuyuki Kanda[1]

[1]*Department of Physics, Osaka City University, Sugimoto 3-3-138, Sumiyoshi, Osaka 558-8585, Japan*
[2]*KAGRA Observatory, Institute for Cosmic Ray Research, University of Tokyo, 238 Higashi Mozumi, Kamioka, Hida, Gifu 506-1205, Japan*
[3]*Gravitational Wave Project Office, National Astronomical Observatory of Japan, 2-21-1, Osawa, Mitaka, Tokyo 181-8588, Japan*
[4]*The Institute of Statistical Mathematics, 10-3 Midori-cho, Tachikawa, Tokyo 190-8562, Japan*
[5]*Laboratoire d'Annecy-le-Vieux de Physique des Particules (LAPP), Université Savoie Mont Blanc, CNRS/IN2P3, F-74941 Annecy-le-Vieux, France*

(Received 15 February 2016; published 29 August 2016)

Noise hunting is a critical requirement for realizing design sensitivity of a detector, and consequently, noise origins and its features have been revealed partially. Among the noise sources to be hunted, sources of nonlinearly correlated noise, such up-conversion noise, are hard to find and can limit the sensitivity of gravitational wave searches with advanced detectors. We propose using a correlation analysis method called maximal information coefficient (MIC) to find both nonlinear and linear correlations. We apply MIC to the scattered light noise correlated between the seismic activity and the strain signal, which limited the sensitivity of the Virgo detector during the first science run. The results show that MIC can find nonlinearly correlated noise more efficiently than the Pearson correlation method. When the data is linearly correlated, the efficiency of the Pearson method and MIC is comparable. On the other hand, when the data is known to be nonlinearly correlated, MIC finds the correlation while the Pearson method fails completely.

DOI: 10.1103/PhysRevD.94.042004

I. INTRODUCTION

In the past several decades, the first generation of kilometer-scale laser interferometric gravitational wave (GW) detectors, TAMA [1], GEO [2], LIGO [3], and Virgo [4], have performed observation runs. Using the observational data, searches of GWs from compact binary coalescences with a neutron star and a black hole [5,6], transient GWs from violent astrophysical phenomena such as galactic supernovae [7], continuous GWs from rapid rotated pulsars [8,9], stochastic GW backgrounds arisen by cosmological or astrophysical sources [10,11] have been performed.

At present, second generation GW detectors, such as Advanced LIGO [3], Advanced Virgo [4], and KAGRA [12], are upgrading to improve the sensitivity or are under construction. The first detection of GW was finally achieved by Advanced LIGO detectors and LSC + Virgo data analysis [13]. In addition to improvements of these detectors, the construction of LIGO-India is under consideration in India [14].

While the sensitivity of GW detectors has been limited by fundamental noises such as shot noise, radiation pressure noise, and seismic noise, practically, an astronomical sensitivity has been limited by unknown nonstationary noise sources such as instrumental artifacts and environmental disturbances. It is important for a claim of confident detection of the GW to track as many nonstationary noise origins as possible. In order to characterize the observation data, thousands of physical environmental monitors (PEM) are installed around the GW detectors LIGO and Virgo. At GW detector sites, the noise huntings with PEM channels have been performed to reveal the nonstationary noise origin and its feature. As a result, a number of noise sources have been identified [15–18]. But several nonstationary noises remain not understood.

Most nonstationary noise influences one or more channels. For example, an acoustic noise is generated by an electronic fan around the detector or by an airplane passing close to the detector. The acoustic noise affects the microphone and the GW channel. In order to identify such a noise origin, the correlation of the GW channel with one or more auxiliary channels can be used. The data affected by the nonstationary noise is either removed or tagged by a flag that rejects the GW search result. This veto procedure improved the efficiency of the GW search [15,19–22].

Up-conversion noise is one of the problematic nonstationary noise, which is generated by the up-conversion of low frequency excitations into the GW-sensitive frequency band with a linear as well as a nonlinear correlation [23,24]. A conventional correlation measure, such as the Pearson correlation coefficient [25], is difficult to find the nonlinearly correlated noise, though it is important to identify

*yuzurihara@yukimura.hep.osaka-cu.ac.jp

the source of up-conversion noise since its mitigation improves the sensitivity of the detector, reduces the false alarm rate, and increases the confidence of the GW detection.

In this paper, we present the first application of a correlation analysis method for finding a nonlinearly correlated noise between signals of PEM channels and the GW strain signal. As an example of a nonlinearly correlated noise, we briefly review a model of the up-conversion noise which has limited the Virgo detector before the second Virgo science run [24]. In this noise model, the laser light is scattered by microseismic activity. The GW channel affected by this backscattered noise is nonlinearly coupled with the seismic noise.

In order to show the detection efficiencies of the correlation analysis methods, we generate simulated data where the seismic noise and the GW strain signal are correlated following the up-conversion noise model.

The paper is organized as follows. In Sec. II, methods for identifying a linear and a nonlinear correlation are briefly described. Section III is a brief review of the up-conversion noise model. Section IV describes the analyzed results and the detection efficiency of the methods. Section V presents a summary of this paper.

II. CORRELATION ANALYSIS

In standard operations of GW detectors, PEM channels are used to monitor the environment of the detector and the status of the interferometer. As introduced in Sec. I, depending on the noise contamination path, an externally induced noise typically produces a correlation between multiple channels. In this section, we describe two methods to find linear and nonlinear correlations between the signal of PEM channels and the GW strain signal.

A. Pearson correlation coefficient

The Pearson correlation coefficient (for short, the Pearson method) of a discrete data set $(x_1, y_1), .., (x_N, y_N)$ is defined as [25]

$$\rho = \frac{\sum_{i=1}^{N}(x_i - \bar{x})(y_i - \bar{y})}{\sqrt{\sum_{i=1}^{N}(x_i - \bar{x})^2}\sqrt{\sum_{i=1}^{N}(y_i - \bar{y})^2}}, \tag{1}$$

where $\bar{x} = N^{-1}\sum_{i=1}^{N} x_i$ and $\bar{y} = N^{-1}\sum_{i=1}^{N} y_i$ are the means. The Pearson method measures a linearity between the data. By contrast, if the data is correlated nonlinearly, such as an X-shape or a sinusoidal shape shown in Fig. 2 of [26], the correlation coefficient is nearly zero. The Pearson method is effective to find a linear relationship but not to respond to a nonlinear relationship. In this paper, "correlation" implicitly assumes a linear dependence.

B. Maximal information coefficient

Recently, methods to find the correlations nonlinearly as well as linearly were proposed [26–29]. In this study, we focus on a maximal information coefficient (MIC) method [26,30].

To calculate MIC, we introduce mutual information. The mutual information $I(s;t)$ of two continuous variables s and t, which are drawn from a joint probability distribution $p(s,t)$, is defined as

$$I(s;t) = \iint dsdtp(s,t)\log_2\frac{p(s,t)}{p(s)p(t)}, \tag{2}$$

where $p(s)$ and $p(t)$ are marginal probability density functions of $p(s,t)$.

Figure 1 shows an example of placement of the grids. In order to calculate the mutual information of discrete data $(x_1, y_1), ..(x_N, y_N)$, rectangular grids are placed with R intervals in the row direction and C intervals in the column direction. All data fall somewhere in the grids.

The mutual information $I(R,C)$ of discrete data $(x_1, y_1), ..(x_N, y_N)$ is defined as

$$I(R,C) = \sum_{r=1}^{R}\sum_{c=1}^{C} p(r,c)\log_2\frac{p(r,c)}{p(r)p(c)}, \tag{3}$$

where the joint probability mass function $p(r,c)$ is estimated by the ratio of $b(r,c)$ to the number of all samples N and $b(r,c)$ is the number of data assigned in rth and cth interval. The marginal probability density $p(r)$ and $p(c)$ is defined as

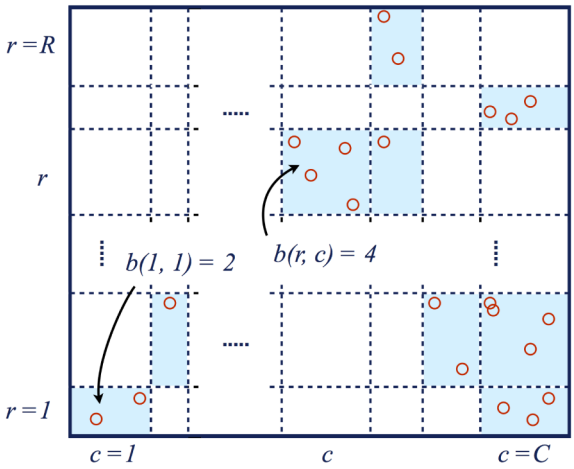

FIG. 1. An example of placed rectangular grids. All discrete data fall somewhere in the grids. The circles represent the discrete data. The dotted lines represents the grids to separate the data. The data are in the shaded regions. The mutual information of the discrete data is calculated by the ratio of $b(r,c)$ to the number of all samples N.

$$p(r) = \sum_{c=1}^{C} p(r,c), \tag{4}$$

$$p(c) = \sum_{r=1}^{R} p(r,c). \tag{5}$$

MIC of the discrete data $(x_1, y_1), ..(x_N, y_N)$ is defined as follows [26,30],

$$\mathrm{MIC}(x,y) = \max_{RC<B(N)} \frac{I(R,C)}{\log_2(\min\{R,C\})}, \tag{6}$$

where $R \geq 2$, $C \geq 2$, $B(N)$ is a maximal number of cells of the grids, and in this study, we estimate MIC with $B(N) = N^{0.6}$ [26,30]. MIC is defined as the statistics maximized under all the possible grids with $RC < B(N)$ because a calculated $I(R,C)$ depends on the number of cells of the grid.

By the definition of mutual information, $I(R,C) \in [0, \log_2(\min\{R,C\})]$ for all R and C, so $\mathrm{MIC}(x,y) \in [0,1]$. If the data are statistically independent, $\mathrm{MIC}(x,y) \to 0$ as $N \to \infty$. On the other hand, if x and y are dependent, $\mathrm{MIC}(x,y) \to 1$ as $N \to \infty$.

III. APPLICATION OF OUR METHOD TO UP-CONVERSION NOISE

In this section, we introduce a noise model of the up-conversion noise [24]. Following this noise model, we generate a set of the simulated up-conversion noise by changing the magnitudes of the induced noise.

A. Correlated noise in the past observations

At the Virgo detector, optical benches are installed at the laser input port, the laser output port, and behind end mirrors, which transmit a tiny fraction of the laser to control the detector. Because the resonance of the optical benches is excited by seismic activity, the scattered light is modulated by the motion of the optical components. This scattered light then recombines with the main optical beam and appears as a phase noise in the GW strain signal. This phase noise $\phi_{\mathrm{sc}}(t)$ can be expressed as [24]

$$\phi_{\mathrm{sc}}(t) = \frac{4\pi}{\lambda}(x_0 + x_{\mathrm{sc}}(t)), \tag{7}$$

where λ is an optical wavelength, x_0 is a static optical path length, and $x_{\mathrm{sc}}(t)$ is a displacement of optical components along the direction of the beam.

There is a correlation between the vibration of the optical component on the bench $x_{\mathrm{sc}}(t)$ and the strain signal $s(t)$ because the phase noise is mixed in $s(t)$ as [24],

$$\begin{aligned} s(t) &= n(t) + n_{\mathrm{sc}}(t) \\ &= n(t) + G \sin\left[\frac{4\pi}{\lambda}(x_0 + x_{\mathrm{sc}}(t))\right], \end{aligned} \tag{8}$$

where $n(t)$ is a fundamental noise of the interferometer, the coupling factor G is a constant defined as $G = T\frac{\lambda}{4\pi}\frac{1}{L}\sqrt{f_{\mathrm{sc}}}$, T is the transmission factor of the cavity end mirrors, L is the arm length of the interferometer, and f_{sc} is a ratio of the transmitted beams to the beams backscattered and re-coupled to the optical field of Fabry-Perot.

The relationship between $x_{\mathrm{sc}}(t)$ and $n_{\mathrm{sc}}(t)$ can be classified in terms of the magnitudes of bench displacements. If the bench displacement is $x_{\mathrm{sc}}(t) \ll \frac{\lambda}{4\pi} \simeq 10^{-7}$ [m], the term in Eq. (8) is approximated as $n_{\mathrm{sc}}(t) \propto G\frac{4\pi}{\lambda}x_{\mathrm{sc}}(t)$, and so, $x_{\mathrm{sc}}(t)$ and $n_{\mathrm{sc}}(t)$ are in a linear relationship. The strain signal is not affected by the scattered light in this case because the contribution of scattering light noise is negligible compared to the detector noise. If the magnitude of the bench displacement is $x_{\mathrm{sc}}(t) \geq 10^{-7}$ [m], $x_{\mathrm{sc}}(t)$ and $n_{\mathrm{sc}}(t)$ are nonlinear correlated and the up-conversion of the scattered light noise occurs.

B. Generation of simulated up-conversion noise

We generate a set of simulated data containing the up-conversion noise by changing the magnitudes of the induced noise. A sampling frequency and a duration of the simulation data are $f_{\mathrm{s}} = 1024$ [Hz] and $T = 1.0$ [s], respectively, and so, the number of the data is $N = 1024$.

The bench displacement $x_{\mathrm{sc}}(t)$ contains the externally induced noise and the bench displacement $x_{\mathrm{seis}}(t)$ as

$$x_{\mathrm{sc}}(t) = A_{\mathrm{m}} \sin(2\pi f_{\mathrm{m}} t) \exp\left(-\frac{t}{\tau}\right) + x_{\mathrm{seis}}(t), \tag{9}$$

where A_{m} is an amplitude (in meters) of the externally induced noise, τ is an attenuation factor, and f_{m} is a resonant frequency of the optical bench. In this study, we use $\tau = 0.1$ [sec] and $f_{\mathrm{m}} = 15$ [Hz] to mimic the up-conversion noise in the Virgo detector. Note that the analysis methods applied in this study are available for realizations with other parameters. We consider the case where $x_{\mathrm{sc}}(t)$ is generated by the externally induced transient event. Note that MIC is even more efficient in the case of a continuous seismic noise exciting scattered light noise.

The time series of the bench displacement is calculated by the inverse Fourier transform to the randomized spectrum as

$$x_{\mathrm{seis}}(t) = \int 10^{-8} \times f^{-2} \tilde{g}(f) e^{2\pi i f t} df, \tag{10}$$

where $\tilde{g}(f)$ is the complex number of which the real and the imaginary part are randomized by Gaussian random numbers, and we assume that the spectrum of the bench displacement follows the power law [31].

Figure 2 shows the randomized spectra of noise components, which are based on the noise budget of the Virgo detector [32]. The time series of the fundamental

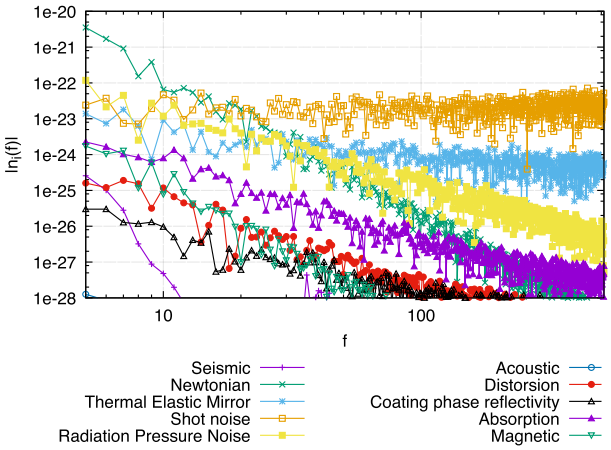

FIG. 2. The spectrum of noise components of Virgo detector [32] which is used to generate the simulated strain signal.

noise $n(t)$ in Eq. (8) is calculated by the inverse Fourier transform to the randomized spectrum as

$$n(t) = \int \tilde{n}(f) e^{2\pi i f t} df, \tag{11}$$

where the coupling factor $G = 5.0 \times 10^{-20}$ as a measured typical value [24], and the optical wavelength $\lambda = 1064$ [nm]; $\tilde{n}(f) = \sum_{i=1}^{10} |n_i(f)| \tilde{g}(f)$, and the each randomized spectrum $|n_i(f)|\tilde{g}(f)$ is shown in Figure 2.

We perform whitening of the strain signal using the averaged spectrum $S_{\rm n}(f)$. A whitened strain signal $w(t)$ is calculated from $s(t)$ as

$$w(t) = \int \frac{\tilde{s}(f)}{\sqrt{S_{\rm n}(f)}} e^{2\pi i f t} df, \tag{12}$$

where $\tilde{s}(f) = \int s(t) e^{-2\pi i f t} dt$, and here, we use $S_{\rm n}(f) = (\sum_{i=1}^{10} |n_i(f)|)^2$.

Figure 3 shows examples of the whitened spectrums of the strain signal. The case of $A_{\rm m} = 0$ has no effect on the up-conversion noise. As the amplitude increases from $A_{\rm m} = 1 \times 10^{-9}$ to $A_{\rm m} = 2 \times 10^{-8}$, the shape of the scattering shoulder appears in the whitened spectrums. The case of $A_{\rm m} = 2 \times 10^{-7}$ and $A_{\rm m} = 4 \times 10^{-7}$ correspond to the situation where the up-conversion noise is stronger than a stable operation. For this reason, we confirmed that the procedure to generate a set of the simulated noise mimic the up-conversion noise in the Virgo detector [24].

Figure 4 shows examples of the simulated data set $x_{\rm sc}(t)$ and $w(t)$. In the case of $A_{\rm m} = 0.0$ and $A_{\rm m} = 1 \times 10^{-9}$, significant structures in the scatter plots are not observed. In the case of $A_{\rm m} = 4 \times 10^{-9}$ and $A_{\rm m} = 2 \times 10^{-8}$, two main components can be seen. The diagonal structure is the effect of the up-conversion noise, and the vertical structure is caused by the background distribution of $x_{\rm sc}(t)$. The scatter plots of $A_{\rm m} = 2 \times 10^{-7}$ and $A_{\rm m} = 4 \times 10^{-7}$ show a sinusoidal shape as expected in Eq. (8).

IV. RESULT OF APPLICATION OF OUR METHOD

We simulate the detection of the nonlinearlity by using the Pearson and MIC methods. The procedure of the simulation is as follows: First, we generate a set of

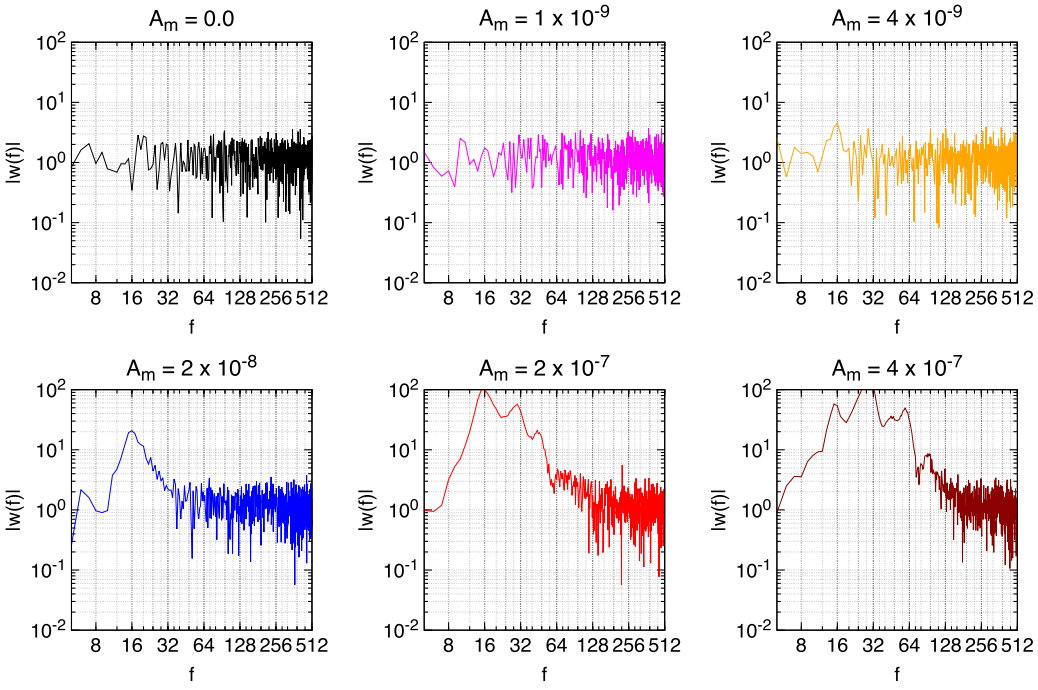

FIG. 3. An example of the whitened spectra $w(f)$ for various values of externally induced noise amplitude $A_{\rm m}$.

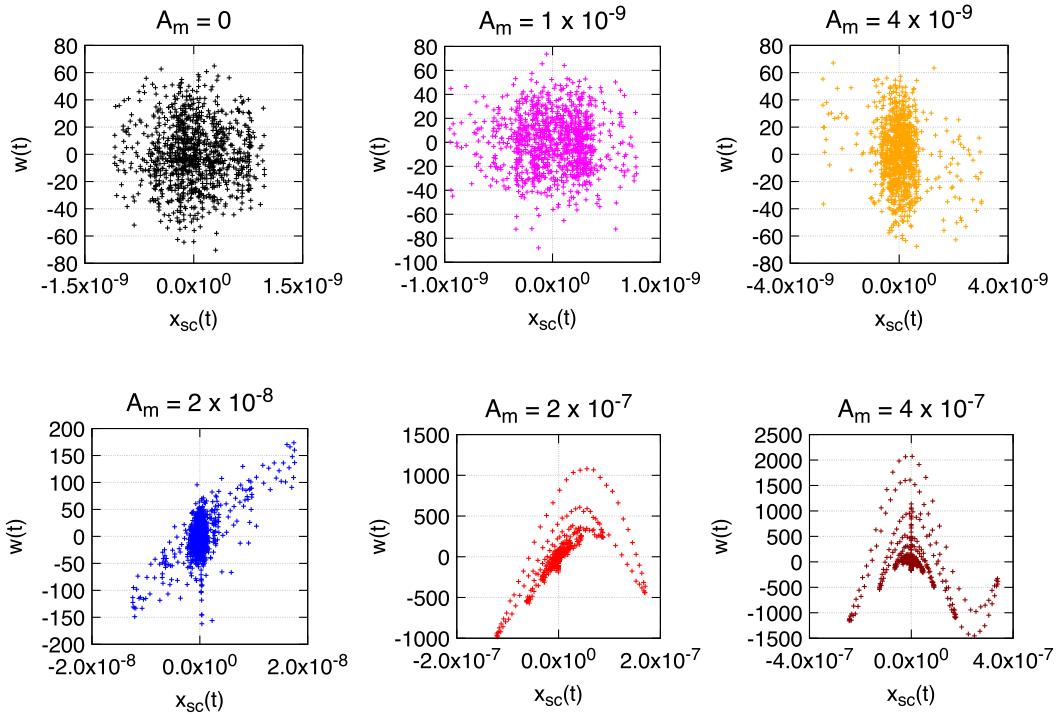

FIG. 4. The scatter plots of the whitened strain signal $w(t)$ versus the bench displacement $x_{sc}(t)$ for various values of the externally induced noise amplitude A_m.

simulated data set $x_{sc}(t)$ and $w(t)$, following the method described in Sec. III B. Second, we obtain transient events by an excess-based method as follows: In this simulation, we assume a simple excess power filter integrating over a frequency domain. The aim of this study is not to find the transient noise but the nonlinear correlation. If we use the time-frequency power map and its clustering, we can increase the detection efficiency of the transient noise. Third, we analyze the triggered data using the correlation analysis methods (MIC and Pearson). Finally, we estimated the efficiency and false alarm probability to detect the up-conversion noise by comparing the data without the up-conversion noise ($A_m = 0$).

We perform the Monte Carlo simulations 10,000 times for each of the following values of the amplitude: $A_m = 1 \times 10^{-9}$, 4×10^{-9}, 2×10^{-8}, 2×10^{-7}, and 4×10^{-7}. The efficiency of each method is evaluated by computing the ratio of the number of events above the threshold to the total number of events. To estimate the background, we generate the simulated data of the amplitude $A_m = 0$, as shown in Figs. 3 and 4. The false alarm probability (FAP) is evaluated as the ratio of the event counts larger than the threshold to the number of the total event counts.

Figure 5 shows a receiver operating characteristic (ROC) curve for each method and each amplitude A_m. Focusing on the Pearson method, in the case of $A_m = 1 \times 10^{-9}$, the

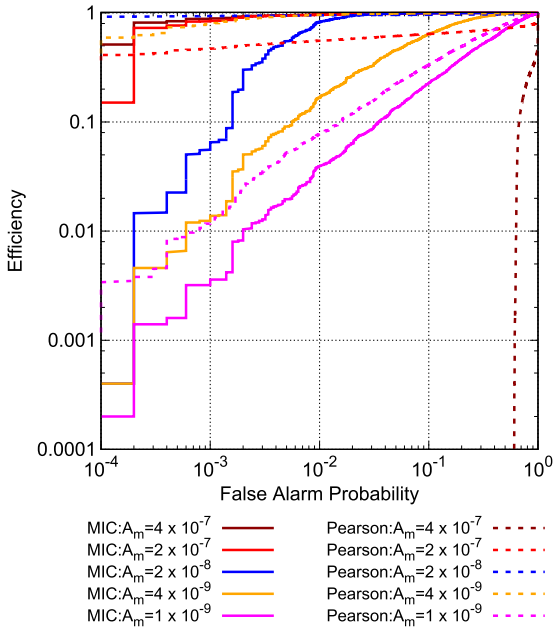

FIG. 5. This graph shows the ROC curve of the Pearson correlation coefficient and MIC with the set of the simulated noise 10,000 times by changing the amplitude of induced noise. The false alarm probability is along the x-axis, and the efficiency is along the y-axis. The amplitudes of the bench displacement are chosen as $A_m = 1 \times 10^{-9}$, 4×10^{-9}, 2×10^{-8}, 2×10^{-7}, and 4×10^{-7}.

efficiency of the Pearson method is 0.07 at FAP $= 0.01$ because the magnitude of the bench displacement is comparable to the detector noise, and also, the data set is not correlated (as seen in Fig. 4). In the case of $A_{\mathrm{m}} = 4 \times 10^{-9}$ and $A_{\mathrm{m}} = 2 \times 10^{-8}$, the relationship of the data approaches the linear correlation as the amplitude of the bench displacement increases. As a result, the efficiency of the Pearson method is improved from 0.07 to 0.96 at FAP $= 0.01$. By contrast, in the case of $A_{\mathrm{m}} = 2 \times 10^{-7}$ and $A_{\mathrm{m}} = 4 \times 10^{-7}$, the efficiency of the Pearson method is decreased to 0.56 and less than 10^{-4} at FAP $= 0.01$, respectively, because the relationship of the data set is changed from a linear to a sinusoidal as seen in Fig. 4. This case corresponds to the situation where the up-conversion noise limits the detector sensitivity.

Focusing on MIC, in the case of $A_{\mathrm{m}} = 1 \times 10^{-9}$, the efficiency of MIC is 0.03 at FAP $= 0.01$. As the amplitude of the bench displacement increases from $A_{\mathrm{m}} = 1 \times 10^{-9}$ to $A_{\mathrm{m}} = 2 \times 10^{-7}$, the efficiency of MIC increases monotonically from 0.03 to 0.97 at FAP $= 0.01$. In the case of $A_{\mathrm{m}} = 4 \times 10^{-7}$, the efficiency of MIC is 0.96 at FAP $= 0.01$.

This result shows that MIC is suitable for finding a nonlinear relationship.

V. SUMMARY

In the past operations of GW detectors, the correlated noise between multiple channels participated in preventing the achievement of design sensitivity. Noise investigations with PEM channels have been performed to characterize correlated noise [15–18] and to find the noise contamination path in the case of linear or nonlinear correlations.

Focusing on the nonlinearly correlated noise, this paper introduced the maximum information coefficient [26,30] and showed that this method can be efficient in finding the seismic nonlinear correlation with the GW strain signal. Using simulated data based on Virgo noise of the first science run [24,31–33], we compared the performance of the Pearson method with the MIC method. The result showed that when the data set is linearly correlated, the efficiency of the Pearson method and MIC method is comparable. By contrast, when the data set is nonlinearly correlated as in the case of $A_{\mathrm{m}} = 4 \times 10^{-7}$, the MIC efficiency is 0.96 for a false alarm rate of 0.01 in 10,000 trials, much above the Pearson method efficiency. Although we treated the case of up-conversion noise caused by the scattered light, in general, we can expect MIC to find other families of nonlinearly correlated noises.

ACKNOWLEDGMENTS

H. Y. and K. H. thank Tomotada Akutsu for fruitful discussions. We are thankful to Raffaele Flaminio for encouragements. This work is supported in part by the MEXT Grant-in-Aid for the Scientific Research on Innovative Areas "New Developments in Astrophysics Through Multi-Messenger Observations of Gravitational Wave Sources" (Grant No. 24103005). K. H. would like to thank B. Allen for the warm hospitality during his stay in Hannover and S. D. Mohanty for valuable comments and encouragement. K. H. is thankful to M.-K. Fujimoto for continuing encouragements.

[1] R. Takahashi (TAMA Collaboration), Classical Quantum Gravity **21**, S403 (2004).
[2] H. Grote (LIGO Scientific Collaboration), Classical Quantum Gravity **27**, 084003 (2010).
[3] B. P. Abbott *et al.*, Rep. Prog. Phys. **72**, 076901 (2009).
[4] F. Acernese *et al.*, Classical Quantum Gravity **25**, 114045 (2008).
[5] J. Abadie *et al.*, Phys. Rev. D **85**, 082002 (2012).
[6] J. Aasi *et al.* (LIGO Scientific Collaboration, Virgo Collaboration), Phys. Rev. D **89**, 102006 (2014).
[7] J. Abadie *et al.*, Phys. Rev. D **85**, 122007 (2012).
[8] J. Aasi, J. Abadie, B. P. Abbott, R. Abbott, T. Abbott, M. R. Abernathy, T. Accadia, F. Acernese, C. Adams, T. Adams *et al.*, Astrophys. J. **785**, 119 (2014).
[9] J. Aasi, B. P. Abbott, R. Abbott, T. Abbott, M. R. Abernathy, F. Acernese, K. Ackley, C. Adams, T. Adams, P. Addesso *et al.*, Phys. Rev. D **91**, 062008 (2015).
[10] J. Aasi *et al.* (LIGO Collaboration, Virgo Collaboration), Phys. Rev. Lett. **113**, 231101 (2014).
[11] J. Aasi *et al.*, Phys. Rev. D **91**, 022003 (2015).
[12] Y. Aso, Y. Michimura, K. Somiya, M. Ando, O. Miyakawa, T. Sekiguchi, D. Tatsumi, and H. Yamamoto, Phys. Rev. D **88**, 043007 (2013).
[13] Abbott *et al.* (LIGO Scientific and Virgo Collaborations), Phys. Rev. Lett. **116**, 061102 (2016).
[14] C. U. S. D. B. Iyer and T. Souradeep, LIGO Report No. LIGO-M1100296-v2.
[15] N. Christensen (LIGO Scientific and Virgo Collaborations), Classical Quantum Gravity **27**, 194010 (2010).
[16] M. W. Coughlin (LIGO Scientific and Virgo Collaborations), Classical Quantum Gravity **28**, 235008 (2011).
[17] J. Aasi, J. Abadie, B. Abbott, R. Abbott, T. D. Abbott, M. Abernathy, T. Accadia, F. Acernese, C. Adams, T. Adams *et al.*, Classical Quantum Gravity **29**, 155002 (2012).
[18] A. Effler, R. M. S. Schofield, V. V. Frolov, G. Gonzâlez, K. Kawabe, J. R. Smith, J. Birch, and R. McCarthy, Classical Quantum Gravity **32**, 035017 (2015).
[19] J. R. Smith, T. Abbott, E. Hirose, N. Leroy, D. MacLeod, J. McIver, P. Saulson, and P. Shawhan, Classical Quantum Gravity **28**, 235005 (2011).

[20] T. Isogai (LIGO Scientific and Virgo Collaboration), J. Phys. Conf. Ser. **243**, 012005 (2010).
[21] P. Ajith, T. Isogai, N. Christensen, R. X. Adhikari, A. B. Pearlman, A. Wein, A. J. Weinstein, and B. Yuan, Phys. Rev. D **89**, 122001 (2014).
[22] C. A. Costa and C. V. Torres, Classical Quantum Gravity **29**, 205018 (2012).
[23] D. Ottaway, P. Fritschel, and S. Waldman, Opt. Express **20**, 8329 (2012).
[24] T. Accadia *et al.*, Classical Quantum Gravity **27**, 194011 (2010).
[25] K. Pearson, Proc. R. Soc. London **58**, 240 (1895).
[26] D. N. Reshef, Y. A. Reshef, H. K. Finucane, S. R. Grossman, G. McVean, P. J. Turnbaugh, E. S. Lander, M. Mitzenmacher, and P. C. Sabeti, Science **334**, 1518 (2011).
[27] G. J. Szkely and M. L. Rizzo, Ann. Appl. Stat. **3**, 1236 (2009).
[28] A. Luedtke and L. Tran, arXiv:1308.5712.
[29] A. Gretton, O. Bousquet, A. Smola, and B. Schlkopf, in *Algorithmic Learning Theory*, Lecture Notes in Computer Science, Vol. 3734, edited by S. Jain, H. Simon, and E. Tomita (Springer, Berlin Heidelberg, 2005), pp. 63–77.
[30] D. N. Reshef *et al.*, Science (2011), http://science.sciencemag.org/content/suppl/2011/12/14/334.6062.1518.DC1.
[31] F. Acernese *et al.*, Classical Quantum Gravity **21**, S433 (2004).
[32] M. Punturo, Report No. VIR-NOT-PER-1390-51, http://w3-1.virgo-gw.eu/senscurve/.
[33] F. Acernese *et al.*, Classical Quantum Gravity **25**, 184003 (2008).